Computers & Fluids 71 (2013) 297–305

Contents lists available at SciVerse ScienceDirect

Computers & Fluids

journal homepage: www.elsevier.com/locate/compfluid

On the combined effects of slip, compressibility, and inertia on the Newtonian extrudate-swell flow problem

Zacharias Kountouriotis [a], Georgios C. Georgiou [a,*], Evan Mitsoulis [b]

[a] Department of Mathematics and Statistics, University of Cyprus, P.O. Box 20537, 1678 Nicosia, Cyprus
[b] School of Mining Engineering & Metallurgy, National Technical University of Athens, Zografou, 157 80 Athens, Greece

ARTICLE INFO

Article history:
Received 9 June 2012
Received in revised form 18 September 2012
Accepted 21 September 2012
Available online 15 November 2012

Keywords:
Extrudate swell
Newtonian fluid
Slip
Compressibility
Inertia
Excess pressure losses
Exit correction
Stability

ABSTRACT

We solve both the planar and axisymmetric extrudate-swell flows of a compressible Newtonian liquid with Navier slip at the wall, using the finite-element method in space and a fully-implicit finite-difference scheme in time. Our aim is to investigate the combined effects of compressibility, slip, and inertia on the shape of the extrudate and the extra pressure losses in the system (exit correction factor). The numerical simulations show that compressibility at moderate and higher Reynolds numbers results in stable steady-state solutions in which the extrudate surface is wavy, especially just after the die exit. The stability of these oscillatory steady-states is investigated by means of time-dependent calculations. At moderate Reynolds and slip numbers, interesting oscillatory extrudate shapes are observed due to the fact that slip tends to reduce the extrudate contraction opposing the inertia effect. The final extrudate swell ratios obtained at high Reynolds numbers and various slip numbers agree well with the theoretical asymptotic values for the case of incompressible flow.

1. Introduction

The role of wall slip in extrusion and other flows has been emphasized in many, mostly experimental studies over the past 60 years [1–4] and has been reviewed by Denn [5] and, more recently, by Hatzikiriakos [6]. Slip is usually associated with complex fluids. However, Newtonian fluids may also exhibit slip, and this phenomenon is of interest in the fields of microfluidic and microeletromechanical devices, as pointed out by Neto et al. [7], who reviewed experimental studies on the slip of Newtonian liquids at solid interfaces.

It is well established that the jet swells at low Reynolds numbers and contracts at moderate and higher Reynolds numbers. Slip tends to reduce swelling in the former and contraction in the latter case. Silliman and Scriven [8] were the first to carry out numerical simulations of Newtonian extrusion using the Navier slip condition instead of the traditional no-slip condition. They concluded that slip at the wall reduces extrudate swell (at low Reynolds numbers), might produce yet larger effects for non-Newtonian liquids, and alleviates the apparent stress singularity at the die exit. Subsequent studies include those of Phan-Thien [9], Georgiou and Crochet [10,11], Mitsoulis [4], and others.

In viscous liquid flows, compressibility becomes important when a sufficient amount of fluid is subject to high pressures [3,10,11]. Such flows occur in several industrial processes, such as extrusion [3], injection blow molding [12], or in flows involving relatively long tubes, such as in waxy crude oil transport [13]. Weakly compressible flows correspond to low values of the Mach number, which is defined as the ratio of the characteristic speed of the fluid to the speed of sound in the fluid (the incompressibility limit corresponds to zero Mach number). Hatzikiriakos and Dealy [14] noted that although the isothermal compressibility of molten polymers is very small, it can have a dramatic effect on the time required for the pressure to level off in a capillary flow experiment.

Beverly and Tanner [15] were the first to investigate the effect of compressibility in creeping, weakly compressible, extrudate-swell flows of Newtonian as well as Maxwell and Phan-Thien Tanner fluids. They presented preliminary results for both planar and axisymmetric flows indicating that the extrudate-swell ratio decreases slightly with compressibility. Subsequently, Georgiou [16] carried out calculations for zero and low Reynolds numbers for an extended range of compressibility values and reported that swelling is reduced only initially and then increases dramatically to values corresponding to foam extrusion experiments [17]. Taliadorou et al. [18] noted that the minimum of the extrudate-swell ratio is shifted to the left when the simulations are performed in longer capillaries, as more material is compressed. Results for even higher compressibility values have recently been reported by

* Corresponding author. Tel.: +357 22892612.
E-mail address: georgios@ucy.ac.cy (G.C. Georgiou).

0045-7930/$ - see front matter © 2012 Elsevier Ltd. All rights reserved.
http://dx.doi.org/10.1016/j.compfluid.2012.09.026

Mitsoulis et al. [19] but only for the creeping flow in short capillaries with no-slip at the wall.

Compressibility effects become more pronounced in time-dependent flows and/or when combined with slip and inertia. Georgiou and Crochet [10,11] pointed out that compressibility may not considerably affect the steady-state solutions but it changes dramatically the flow dynamics. They considered time-dependent compressible extrudate-swell flow with non-monotonic slip at the wall and used a linear equation of state. They demonstrated numerically that if the volumetric flow rate is in the negative regime of the flow curve, self-sustained oscillations of the pressure drop and of the mass flow rate at the exit are obtained, and the extrudate surface becomes wavy, as is the case with the stick–slip instability in polymer extrusion. The numerical simulations were later extended to include non-Newtonian (e.g. Carreau) fluids and the barrel region [20]. Taliadorou et al. [18] studied the extrudate-swell flow of strongly compressible Newtonian fluids representing foams, using a linear and an exponential equation of state. Their results confirmed once again that, as the compressibility of the fluid is increased, the swelling decreases initially, and then it increases considerably, exhibiting also stable steady-state free surface oscillations for moderate and higher Reynolds numbers. Taliadorou et al. [18] note that oscillatory steady-state solutions are also obtained when the fluid is allowed to slip at the wall.

We have recently reviewed various factors affecting the extrudate-swell flow of a Newtonian fluid issuing from either a planar slit or a circular tube [19]. The effects of inertia, gravity, compressibility, pressure-dependence of the viscosity, slip at the wall, and surface tension have all been investigated individually in parametric studies covering a wide range of the relevant parameters. Since previous studies are mostly concerned with low-Reynolds or even creeping flows, in this paper we study the combined effects of wall slip and compressibility with inertia. Recently, Russo and Phillips [21] pointed out that even though the viscoelastic extrudate-swell problem (the mechanism of which is unrelated to the viscoelastic analog) is of higher interest for industrial purposes, the Newtonian extrudate-swell problem also deserves a deep analysis that can provide an important insight into the underlying physics. They also noted that increasing inertia leads to increases of the normal stresses and the normal stress difference while swelling is reduced.

The objective of the present work is to investigate by means of numerical simulations the combined effects of compressibility, slip, and inertia on Newtonian extrudate-swell flow, and report both the extrudate swell or contraction and the excess pressure losses in the system known as exit correction [4]. Special emphasis is given on the oscillatory steady-state solutions at moderate and higher Reynolds numbers when compressibility is taken into account. Their stability is verified by means of time-dependent calculations. Moreover, the asymptotic extrudate-swell ratios in the case of Navier slip at the wall are derived and tested against the numerical simulations.

2. Governing equations

We consider the time-dependent, two-dimensional (2D) planar or axisymmetric extrudate-swell flow of a compressible Newtonian liquid assuming that gravity forces are negligible. Hence, the continuity and momentum equation are as follows:

$$\frac{\partial \rho}{\partial t} + \nabla \cdot (\rho \mathbf{u}) = 0, \tag{1}$$

$$\rho\left(\frac{\partial \mathbf{u}}{\partial t} + \mathbf{u} \cdot \nabla \mathbf{u}\right) = -\nabla p + \nabla \cdot \boldsymbol{\tau}, \tag{2}$$

where $\mathbf{u}$ is the velocity vector, p is the pressure, $\boldsymbol{\tau}$ is the viscous stress tensor, t is the time, and ρ is the density. Under the assumption of zero bulk viscosity, $\boldsymbol{\tau}$ is given by

$$\boldsymbol{\tau} = \mu[(\nabla \mathbf{u}) + (\nabla \mathbf{u})^T] - \frac{2}{3}\mu \mathbf{I} \nabla \cdot \mathbf{u}, \tag{3}$$

where $\boldsymbol{I}$ is the unit tensor, μ is the constant viscosity, and the superscript T denotes the transpose of a tensor. Substituting the viscous stress tensor into the momentum equation, one gets

$$\rho\left(\frac{\partial \mathbf{u}}{\partial t} + \mathbf{u} \cdot \nabla \mathbf{u}\right) = -\nabla p + \mu \nabla^2 \mathbf{u} + \frac{1}{3}\mu \nabla(\nabla \cdot \mathbf{u}), \tag{4}$$

The equations of motion (1) and (4) are completed by an equation of state relating the density to the pressure. In the present work, we use the following *linear* approximation

$$\rho = \rho_0[1 + \beta(p - p_0)], \tag{5}$$

where ρ_0 is the density at the reference pressure p_0 and β is the isothermal compressibility, assumed to be the constant defined by

$$\beta \equiv -\frac{1}{V_0}\left(\frac{\partial V}{\partial p}\right)_{p_0,T}, \tag{6}$$

where V is the volume, V_0 is the specific volume at the reference pressure p_0, and T is the temperature.

2.1. Boundary conditions

The geometry and boundary conditions of the axisymmetric extrudate-swell problem are shown in Fig. 1. The standard symmetry conditions for zero radial velocity and shear stress along the axis of symmetry are assumed, i.e. $u_r = 0$ and $\tau_{rz} = 0$. Along the capillary wall, the radial velocity is set to zero (no penetration) and the axial velocity obeys Navier's slip condition [4,19]:

$$u_w = a\tau_w, \tag{7}$$

where u_w is the slip velocity, τ_w is the shear stress at the wall, and a is a slip parameter depending on material properties. The inlet plane is taken at a distance L_1 sufficiently far upstream the exit so that the flow can be taken as fully developed, i.e., $u_r = 0$ and

$$u_z = \frac{1}{4\mu}\left(-\frac{\partial p}{\partial z}\right)R^2\left[1 - \left(\frac{r}{R}\right)^2 + \frac{2\mu a}{R}\right] \tag{8}$$

where $(-\partial p/\partial z)$ is the pressure gradient.

At a plane taken at a distance L_2 sufficiently far from the die exit so that the flow can be considered uniform, the total normal stress and the shear stress are assumed to vanish, $-p + \tau_{zz} = 0$ and $\tau_{rz} = 0$. Finally, on the free surface, it is assumed that surface tension is zero, and vanishing normal and tangential stresses are imposed. Additionally, the kinematic condition is applied:

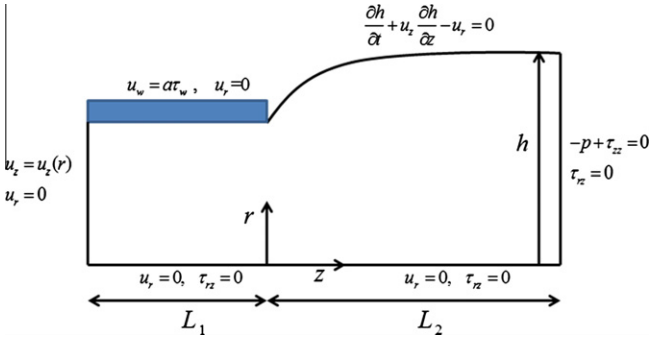

Fig. 1. Geometry and dimensionless boundary conditions for the axisymmetric Newtonian extrudate-swell flow with slip at the wall.

$$\frac{\partial h}{\partial t} + u_z \frac{\partial h}{\partial z} - u_r = 0. \tag{9}$$

where $h(z,t)$ is the position of the free surface.

2.2. Dimensionless equations

The governing equations are non-dimensionalized by scaling the lengths by the radius R of the tube, the velocity vector by the mean velocity U at the inlet of the tube, the time by R/U, the pressure and the stress tensor components by $\mu U/R$, and the density by ρ_0. Hence, the continuity and momentum equations become

$$\frac{\partial \rho^*}{\partial t^*} + \nabla^* \cdot (\rho^* \mathbf{u}^*) = 0, \tag{10}$$

and

$$Re\left(\frac{\partial \mathbf{u}^*}{\partial t^*} + \mathbf{u}^* \cdot \nabla^* \mathbf{u}^*\right) = -\nabla^* p^* + \nabla^{*2} \mathbf{u}^* + \frac{1}{3}\nabla^*(\nabla^* \cdot \mathbf{u}^*), \tag{11}$$

where the stars denote dimensionless variables and

$$Re \equiv \frac{\rho U R}{\mu}, \tag{12}$$

is the Reynolds number. The equation of state (5) becomes

$$\rho^* = 1 + B p^*, \tag{13}$$

where B is the compressibility number

$$B \equiv \frac{\beta \mu U}{R}. \tag{14}$$

The dimensionless form of the slip equation is

$$u_w^* = A \tau_w^*, \tag{15}$$

where

$$A \equiv \frac{a\mu}{R}, \tag{16}$$

is the slip number. De-dimensionalization does not change the expression for the kinematic Eq. (9).

Finally the dimensionless velocity profile imposed at the inlet plane is

$$u_z^* = \frac{2}{1+4A}(1 - r^{*2} + 2A). \tag{17}$$

The governing equations for the planar flow problem are similar. For example, the dimensionless fully-developed velocity imposed at the inlet is

$$u_x^* = \frac{3}{2(1+3A)}(1 - y^{*2} + 2A). \tag{18}$$

2.3. Asymptotic extrudate-swell ratios

The extrudate-swell ratio is defined as the ratio of the final extrudate dimension, h_f, to that of the die. Thus, in the case of the axisymmetric flow, this ratio is defined by

$$\chi^* \equiv \frac{h_f}{R}, \tag{19}$$

For convenience, the stars denoting dimensionless variables are dropped hereafter.

In the case of incompressible flow, the asymptotic limits of the extrudate-swell ratio at infinite Reynolds numbers are estimated by taking mass and momentum balances between the exit of the die, where the flow is assumed to be fully developed, and at the

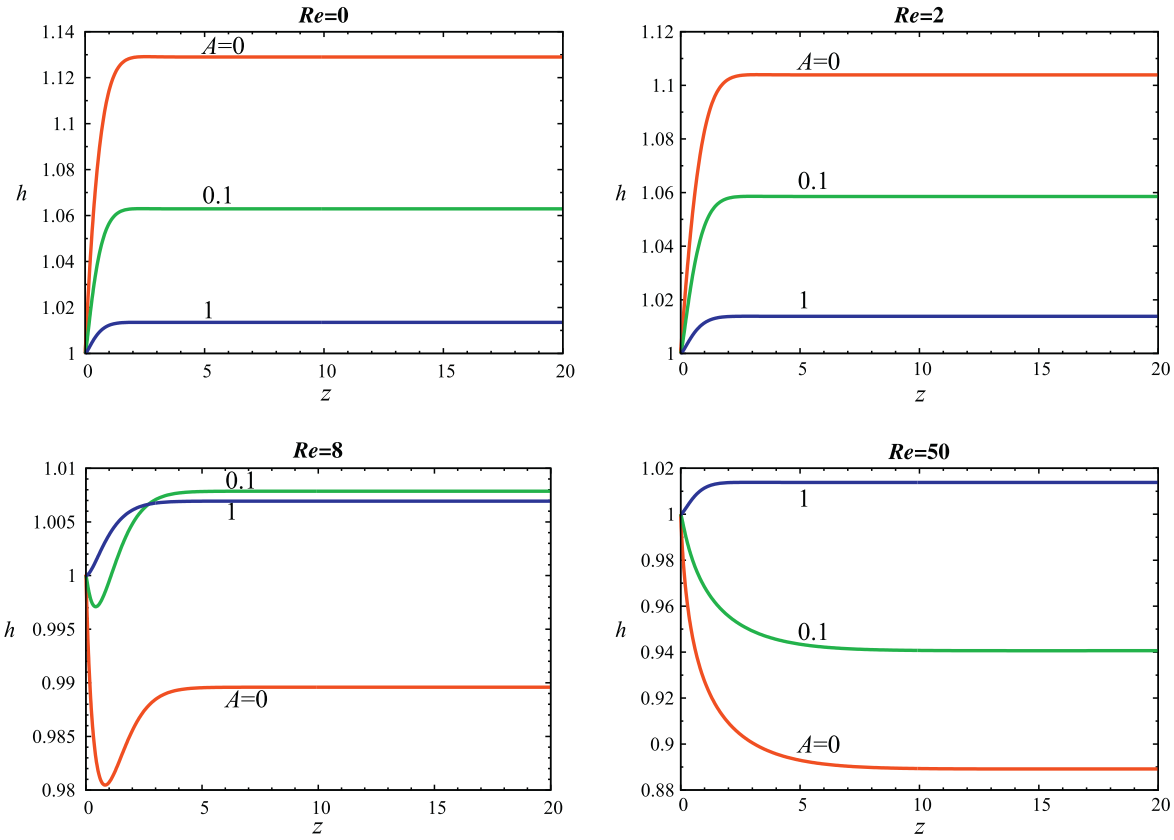

Fig. 2. Free surface profiles in incompressible axisymmetric extrudate-swell flow for various slip numbers and Re = 0, 2, 8, and 50. Note that the y-scale is not the same in all graphs.

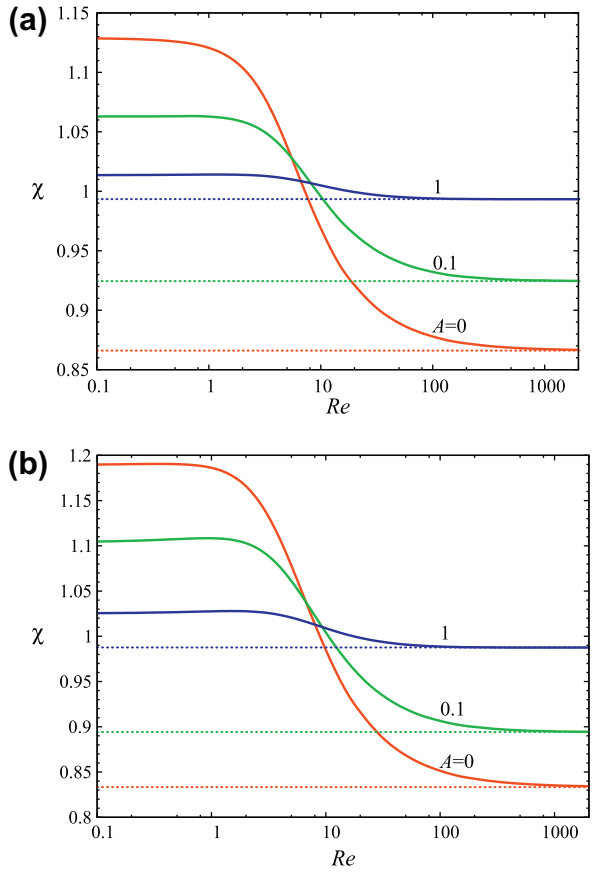

Fig. 3. Extrudate-swell ratio as a function of the Reynolds number in (a) axisymmetric and (b) planar incompressible extrudate-swell flow. The dotted lines indicate the asymptotic limits.

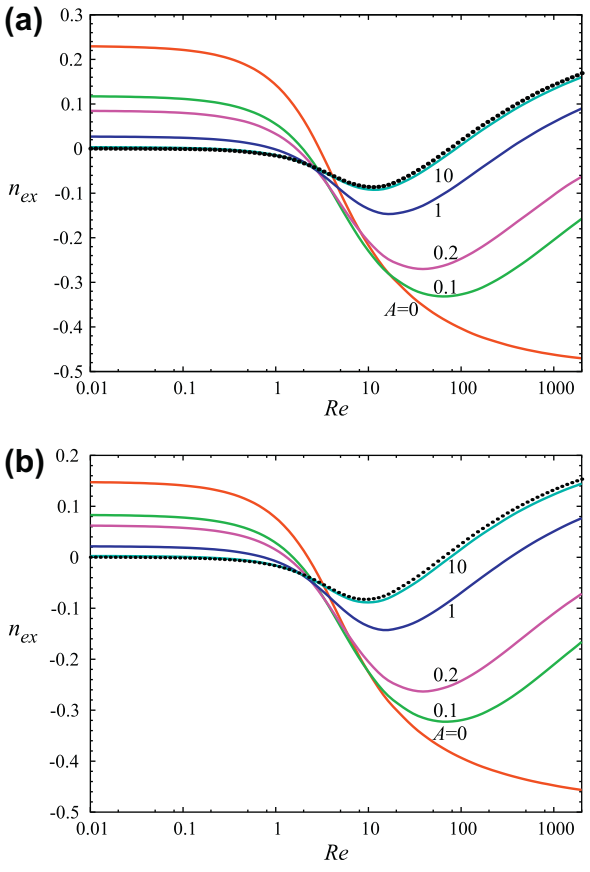

Fig. 4. Exit correction as a function of the Reynolds number in (a) axisymmetric and (b) planar incompressible extrudate-swell flow. The dotted lines indicate the asymptotic limits for full slip.

extrudate region very far downstream where the flow is taken as a plug. After some algebra it is not difficult to show that the asymptotic values of the extrudate-swell ratio for the axisymmetric and planar cases are, respectively,

$$\chi_\infty = \frac{1}{\left[1+\frac{1}{3(1+4A)^2}\right]^{1/2}}, \quad \text{(axisymmetric)} \tag{20}$$

and

$$\chi_\infty = \frac{1}{1+\frac{1}{5(1+3A)^2}}. \quad \text{(planar)} \tag{21}$$

In the case of no slip ($A = 0$), the above expressions yield the asymptotic values of Harmon [22] and Tillett [23], i.e., $\sqrt{3}/2(0.866)$ and 5/6 (0.833), respectively.

3. Numerical method

The Finite Element Method is used for solving the system of governing equations and boundary conditions. The free-surface profile is computed simultaneously with the velocity and pressure fields (u-v-p-h formulation), and the mesh is updated at each iteration step utilizing a spine scheme. Standard biquadratic basis functions are used for the velocity components and bilinear ones for the pressure. Moreover, a quadratic representation is employed for the position h of the free surface. For the spatial discretization, the standard Galerkin forms of the continuity, momentum, and kinematic equations are used, while for the time discretization, the standard fully-implicit (Euler backward difference) scheme has been used. The resulting nonlinear system of discretized equations is solved with the Newton–Raphson iterative scheme with a 10^{-5} tolerance.

The length L_1 of the capillary was taken to be equal to 5. For creeping flow and moderate Reynolds numbers, the length of the extrudate was taken to be $L_2 = 20$. This was increased up to $L_2 = 2000$ for high Reynolds numbers, resolving the problem of high wavelength of the free-surface oscillations present in inertial flows. Mitsoulis et al. [19] recommended setting $L_2 = Re$ for $Re > 20$.

4. Results and discussion

We first investigate the effects of inertia and slip on the incompressible extrudate-swell flows of interest, setting as the base flow that for which $B = Re = A = 0$. We study, in particular, the extrudate swell ratio, χ, and the dimensionless excess pressure losses, commonly known as *exit correction*, n_{ex}, defined as follows [24]:

$$n_{ex} \equiv \frac{\Delta P_w - \Delta P_0}{2\tau_w}, \tag{22}$$

where ΔP_w is the overall pressure drop along the wall, ΔP_0 is the pressure drop based on the fully developed flow in the tube (or in the channel) without the extrudate region, and τ_w is the wall shear stress for fully-developed Poiseuille flow. The exit correction represents the extra pressure that is needed in extrusion due to the exit flow and corresponds to a quantity readily measured in experiments obtained from the overall pressure in the system. It turns out that

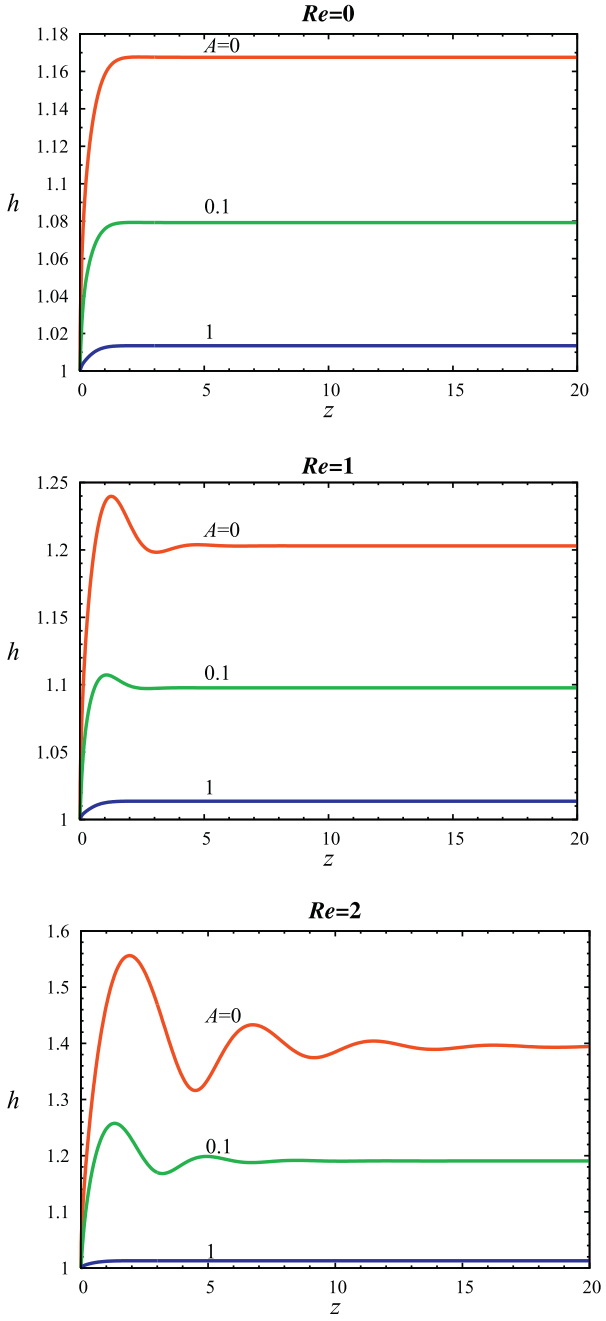

Fig. 5. Free surface profiles in compressible ($B = 0.06$) axisymmetric extrudate-swell flow for various slip numbers and $Re = 0$, 1, and 2. Note that the y-scale is not the same in all graphs.

$$n_{ex} = \frac{(1+4A)\Delta P_w}{8} - L_1 \quad \text{(axisymmetric)}, \tag{23}$$

and

$$n_{ex} = \frac{(1+3A)\Delta P_w}{6} - \frac{L_1}{2} \quad \text{(planar)}. \tag{24}$$

Results in the present work have been obtained for an extended range of Reynolds, compressibility and slip numbers. These ranges are: $0 \leqslant Re \leqslant 2000$, covering the range from inertialess flow to the end of the laminar flow regime; $0 \leqslant B \leqslant 0.06$, covering the range from incompressible flow to very compressible viscous flow; and $0 \leqslant A \leqslant 1$, covering the range of flow with no-slip to macroscopically obvious slip at the wall (almost plug velocity profile).

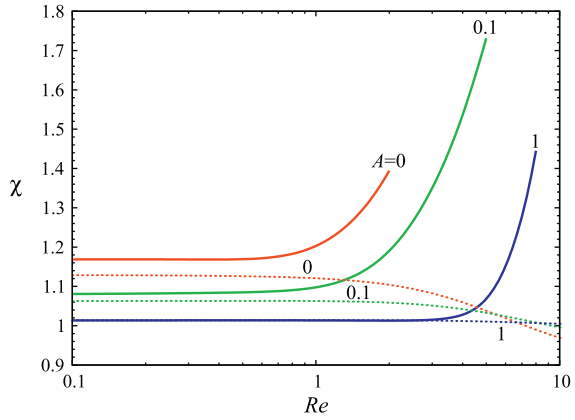

Fig. 6. Final extrudate-swell ratios for various slip numbers in axisymmetric compressible extrudate-swell flow with $B = 0.06$. The dotted lines correspond to incompressible flow ($B = 0$).

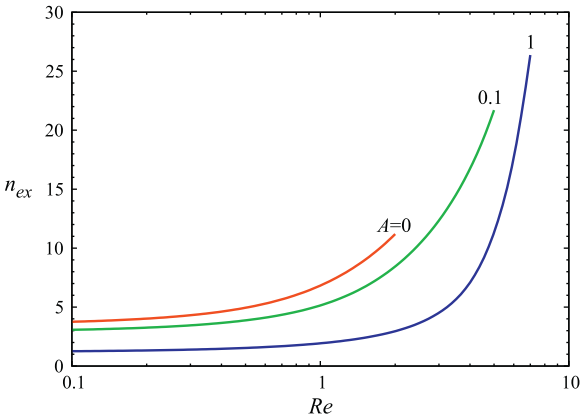

Fig. 7. Exit corrections versus Re for various slip numbers in axisymmetric compressible extrudate-swell flow with $B = 0.06$.

The effects of the slip number on the steady-state incompressible axisymmetric flow for $Re = 0$, 2, 8, and 50 and $L_2 = 50$ are illustrated in Fig. 2. In general, slip tends to reduce swelling at low Reynolds numbers and contraction at higher Reynolds numbers. For moderate Reynolds numbers (e.g., $Re = 8$), the extrudate is characterized by a necking, where the jet contracts initially and then expands. Necking is reduced by slip. In Fig. 3, the calculated extrudate-swell ratios for three different slip number ($A = 0$, 0.1, and 1) are plotted versus the Reynolds number up to $Re = 2000$, i.e., in the laminar regime, for both the axisymmetric and planar flows. The extrudate swell ratio decreases rapidly for $Re > 1$ approaching nicely the asymptotic values given by Eqs. (20) and (21). The exit corrections obtained with the same parameters are plotted versus the Reynolds number in Fig. 4. In the case of no-slip, the exit correction decreases monotonically to zero following a sigmoidal shape, similar to that of the extrudate-swell ratio. For small Reynolds numbers, slip reduces n_{ex} but this trend is reversed at high Reynolds numbers when the exit correction becomes negative. As a result, a local minimum is observed at moderate Reynolds numbers, which is shifted to the left and higher as the slip number is increased.

In order to investigate the combined effects of compressibility and slip on the extrudate-swell ratio we set $B = 0.06$ and considered three slip numbers: $A = 0$, 0.1, and 1. From our previous study [18], it is known that in the compressible case the angle of expansion and the swelling both increase with Reynolds number, and

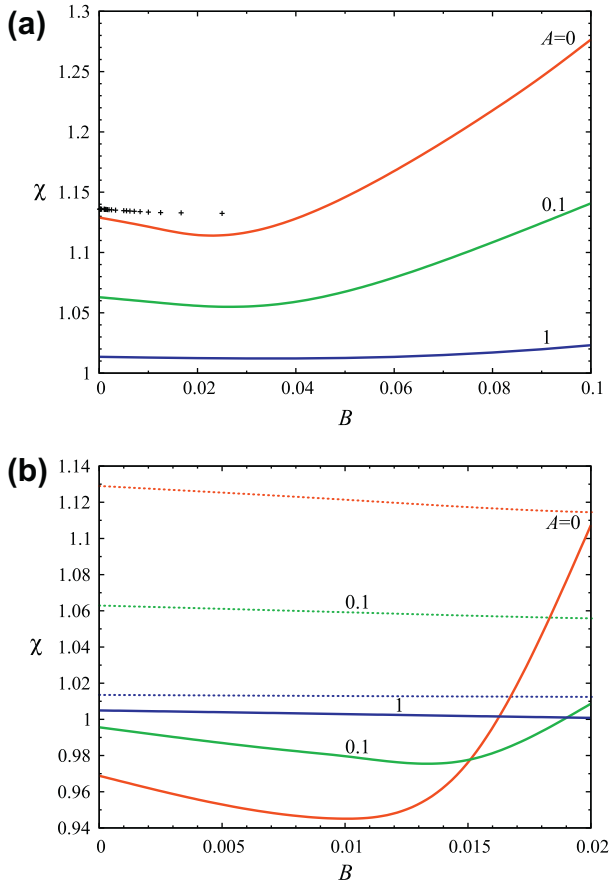

Fig. 8. Axisymmetric extrudate-swell ratio versus the compressibility number for various slip numbers: (a) $Re = 0$; the points (+) are the values provided by Beverly and Tanner [15]; (b) $Re = 10$; note that the range of B is much smaller and the dotted lines are the predictions for $Re = 0$.

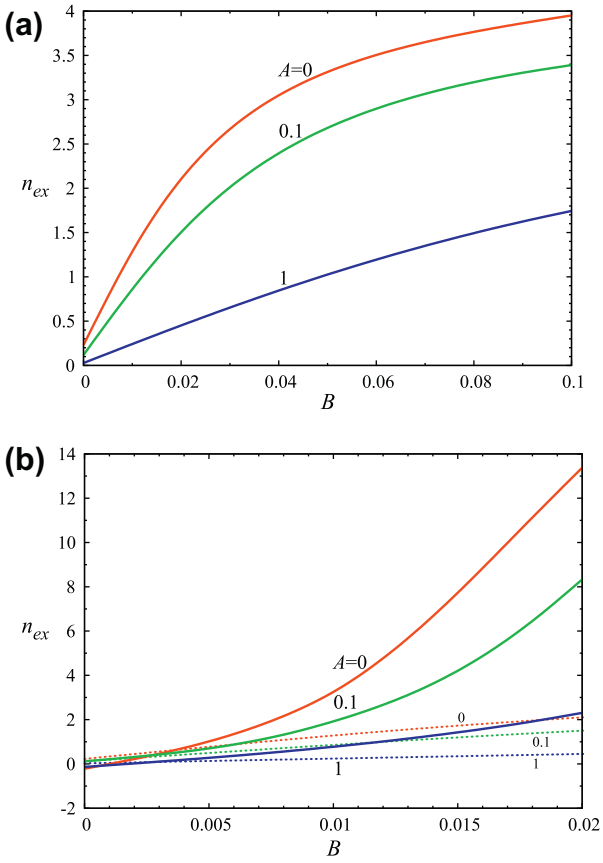

Fig. 9. Exit correction in axisymmetric extrudate-swell flow versus the compressibility number for various slip numbers: (a) $Re = 0$; (b) $Re = 10$; note that the range of B is much smaller and the dotted lines are the results for $Re = 0$.

oscillations appear on the steady-state extrudate surface which decay downstream. The amplitude and the wavelength of these oscillations increase with compressibility. Since for high values of Re the extrudate surface becomes highly oscillatory, computations for the compressible case were restricted to low and moderate Re. As illustrated in Fig. 5, where extrudate surfaces for $Re = 0$, 1, and 2 are shown, slip reduces swelling alleviating the compressibility effects, in agreement with previous studies [18]. Slip also suppresses and eventually eliminates the free surface oscillations observed at moderate Re.

In Fig. 6, we plot the computed extrudate-swell ratios versus Re. The corresponding curves for the incompressible flow are also shown for comparison purposes; these lines lie below their compressible counterparts. While in the incompressible flow swelling is reduced with Re, in the compressible case χ increases sharply after an initial plateau, which explains why only very low Re have been considered for $B = 0.06$. Slip stretches the plateau delaying the sharp increase of χ to higher Re. When slip is strong ($A = 1$) swelling is reduced anyway, and compressibility has no effect on χ for Re roughly less than 3. Similar conclusions can be drawn for the exit correction factor, as illustrated in Fig. 7.

In Fig. 8 we plot the extrudate-swell ratio as a function of the compressibility number for the three representative slip numbers of interest ($A = 0$, 0.1, and 1) and $Re = 0$ and 10. We observe that χ passes through a minimum, which is a well-known effect of compressibility. The results for the creeping flow without slip are the same as those we reported earlier [16,18,19]; the points obtained (with a rather coarse mesh) in the pioneering work of Beverly and Tanner [15] are also shown. It should be noted that a different velocity scale was used in [16], which caused shifting of the minimum to the right. Taliadorou et al. [18] noted that increasing the length of the capillary, and thus the volume of the material that is being compressed, moves the minimum of the extrudate-swell ratio to the left.

In creeping flow, slip reduces swelling and alleviates compressibility effects. However, when the Reynolds number is increased to $Re = 10$ (Fig. 8b), the range of feasible compressibility numbers is reduced considerably, due to the appearance of the steady-state free-surface oscillations. The dotted lines show the corresponding results for the creeping flow ($Re = 0$); in this regime, χ decreases slightly with the compressibility number. The initial reduction of the extrudate-swell ratio is weakened and the local minimum is shifted to the right as the slip number is increased. Finally, at non-zero Re the increase of χ after the minimum becomes faster. Similar results have been obtained for the planar extrudate-swell jet, which is known to swell more than its axisymmetric counterpart below a certain value of the compressibility number [18]. For the ranges of slip and Reynolds numbers examined, the exit correction increases monotonically with compressibility as shown in Fig. 9. As already deduced from Fig. 7, this increase becomes sharper with inertia and less pronounced with wall slip. The curve for $A = 0$ in Fig. 9a coincides with that we presented in [19] but differs from the results in [18] where the exit correction was calculated using the pressure difference along the symmetry axis (instead of the wall).

The combined effects of inertia, compressibility, and slip are also illustrated in Figs. 10 and 11, where the axisymmetric extrudate-swell ratio and the exit correction factor are plotted versus

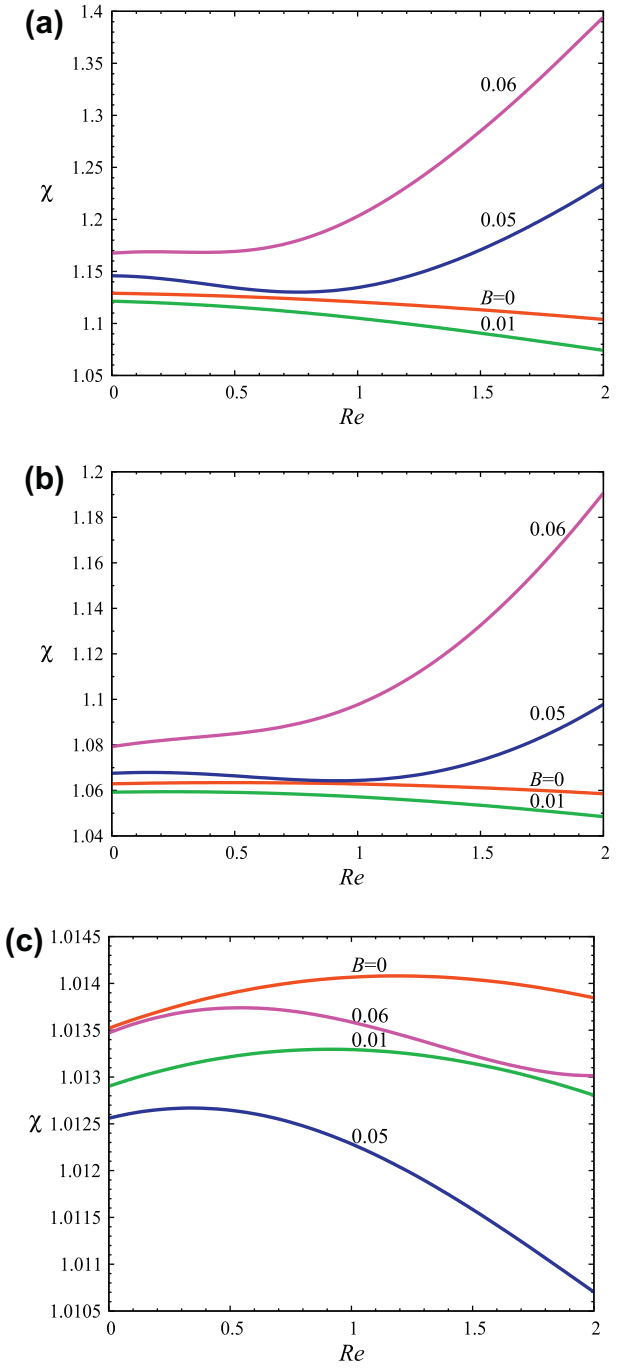

Fig. 10. Axisymmetric extrudate-swell ratio for various compressibility numbers: (a) $A = 0$ (no slip at the wall); (b) $A = 0.1$; (c) $A = 1$.

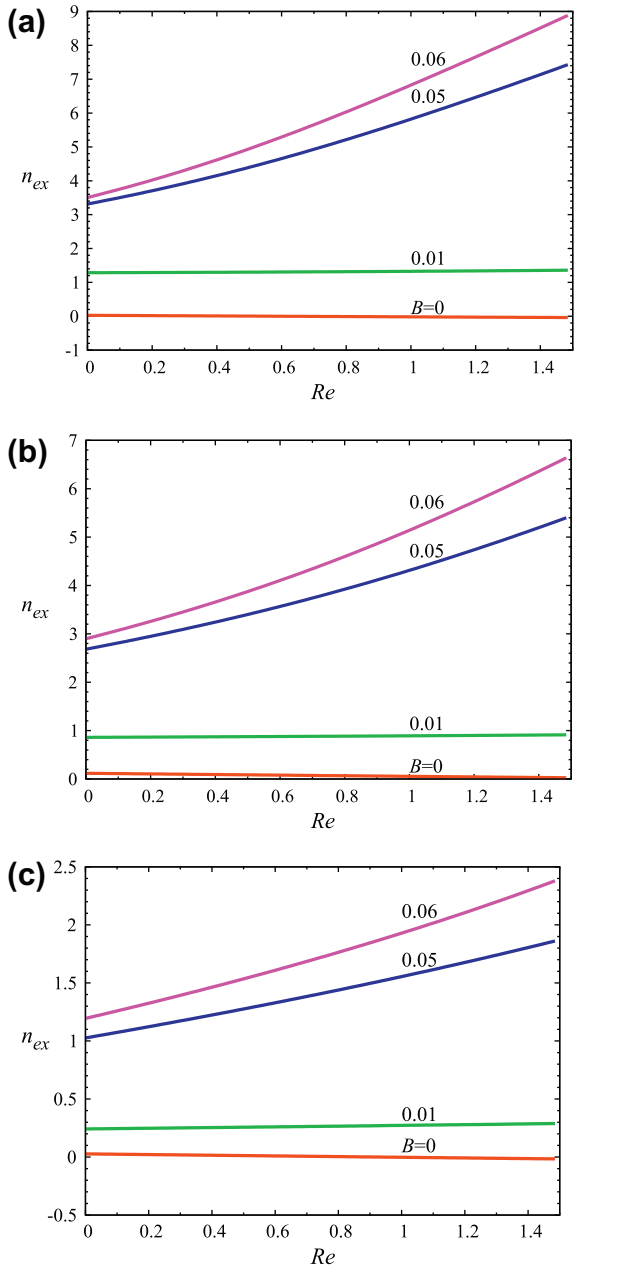

Fig. 11. Exit corrections in axisymmetric extrudate-swell flow for various compressibility numbers: (a) $A = 0$ (no slip at the wall); (b) $A = 0.1$; (c) $A = 1$.

the Reynolds number in the interval [0,2] for different compressibility and slip numbers. In the no-slip case and for small compressibility numbers, χ is a decreasing function of Re, while a minimum is observed for higher values of B. The results in Fig. 10a (no-slip) coincide with those in [18] which reached only up to $Re = 1$. When slip is present (Fig. 10b and c) the range of extrudate-swell ratios is reduced. When slip is strong, χ increases initially and exhibits a maximum.

As already discussed, at low Reynolds numbers increasing the compressibility initially reduces and then enhances swelling (Fig. 8). This effect is also illustrated in Fig. 12a where free-surface profiles for the creeping flow ($Re = 0$) and different compressibility numbers in the no-slip case ($A = 0$) are plotted. A similar trend is observed at low Reynolds numbers. What is interesting, however, is the existence of steady-state solutions in which the free surface is oscillatory. These oscillations seem to decay downstream. For $Re = 5$, the incompressible jet is known to contract initially. Increasing the compressibility initially leads to further contraction and then to swelling accompanied by free-surface oscillations (Fig. 12b). Interesting shapes of the free surface may be obtained for certain combinations of the compressibility and Reynolds numbers. For example, for $Re = 10$ and $B = 0.015$ (Fig. 12c), the free surface contracts slightly after an initial kink. In a certain range of compressibility numbers, the free surface practically exhibits only one or two oscillations just after the die exit, which is consistent with experimental observations. The phenomenon of the contraction of the extrudate after the initial expansion near the die exit is common in extrusion experiments with different materials, e.g. polymer [25] and starch-based [26] foams. Generally speaking, slip

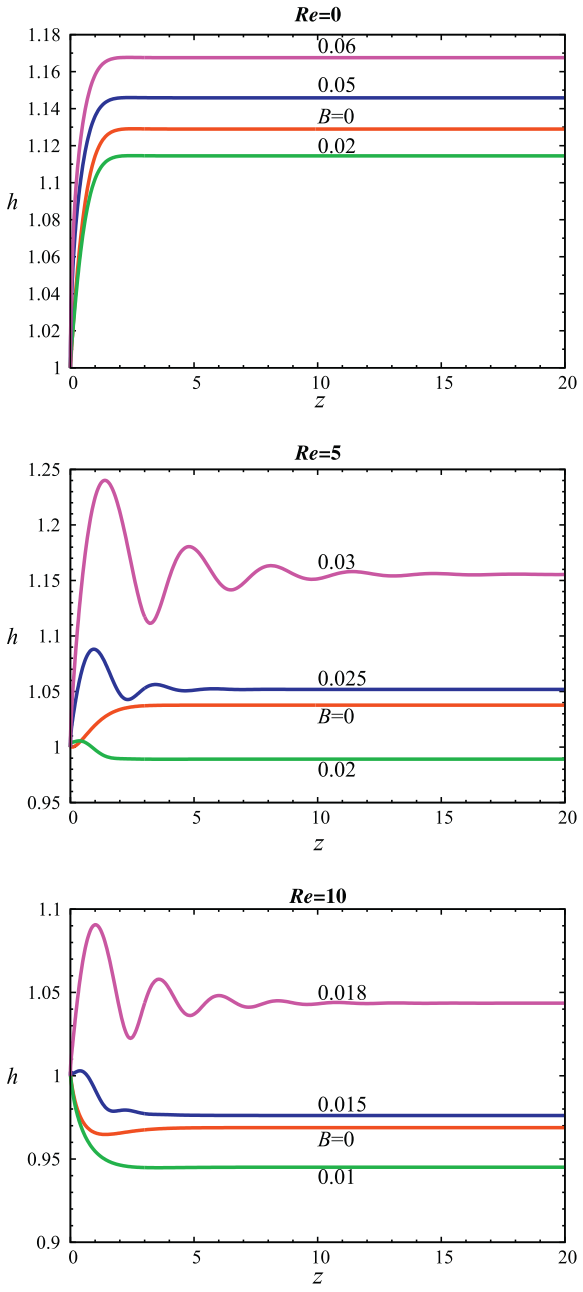

Fig. 12. Free surface profiles in compressible axisymmetric extrudate-swell flow with no slip ($A = 0$) for $Re = 0$, 5, and 10. Note that the y-scale is not the same in all graphs.

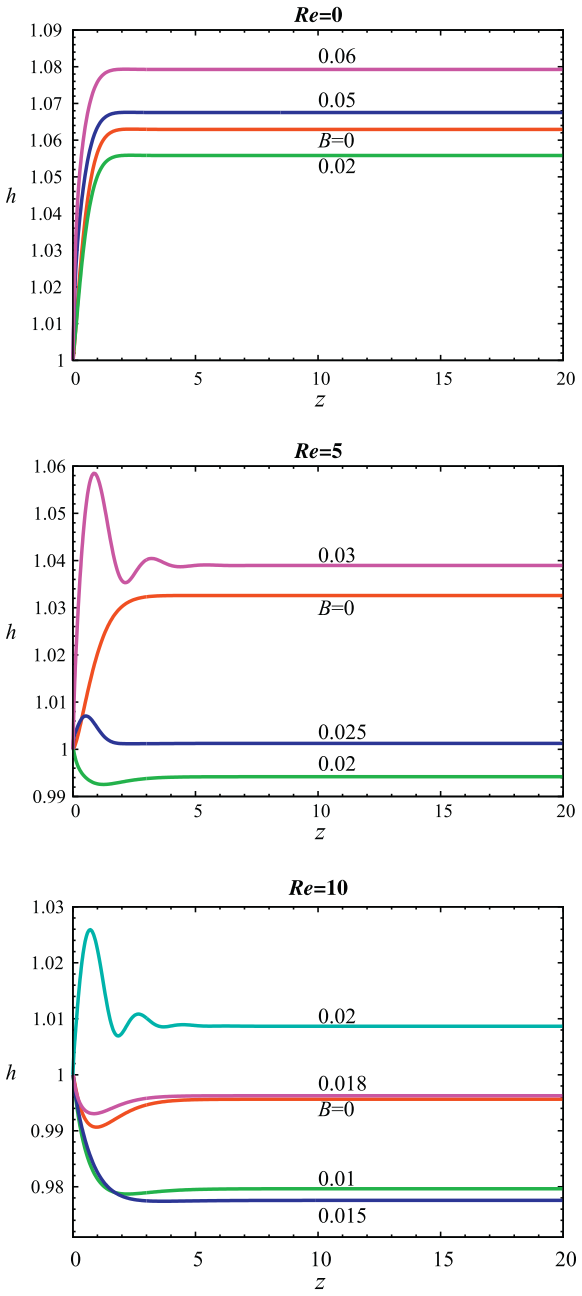

Fig. 13. Free surface profiles in compressible axisymmetric extrudate-swell flow with slip at the wall ($A = 0.1$), for $Re = 0$, 5, and 10. Note that the y-scale is not the same in all graphs.

suppresses both the swelling and the contraction of the extrudate. In the case of compressible flow, it also suppresses the steady-state free surface oscillations, as illustrated in Fig. 13, where the steady-state free-surface profiles for the same Reynolds and compressibility numbers as in Fig. 12 and $A = 0.1$ are plotted.

The stability of the oscillatory steady-state solutions has been investigated by means of time-dependent simulations using meshes with different extrudate lengths. Representative results for $Re = 2$, $B = 0.06$ (very compressible flow), and $A = 0$ (no slip) are illustrated in Fig. 14. The volumetric rate condition was set at $Q_0 = 0.5$ and at $t = 0$ the volumetric flow rate was set to $Q = 1$. An overshoot appears that grows considerably but travels and disappears downstream. Oscillations are then developed on the free surface, and a stable oscillatory solution is finally reached. Time-dependent calculations with slip at the wall (i.e., for nonzero A) showed that, as with the steady-state solutions, wall slip reduces the size of the free-surface oscillations.

5. Conclusions

The combined effects of slip, compressibility, and inertia on the extrudate-swell ratio and the exit correction factor in both the axisymmetric and planar extrudate-swell flows have been analyzed by means of finite-element simulations. We have employed Navier's slip condition and a linear equation of state to relate the density to the pressure. The asymptotic values of the extrudate-swell ratio for the incompressible flow in the presence of slip have been derived. The numerical results indicate the following:

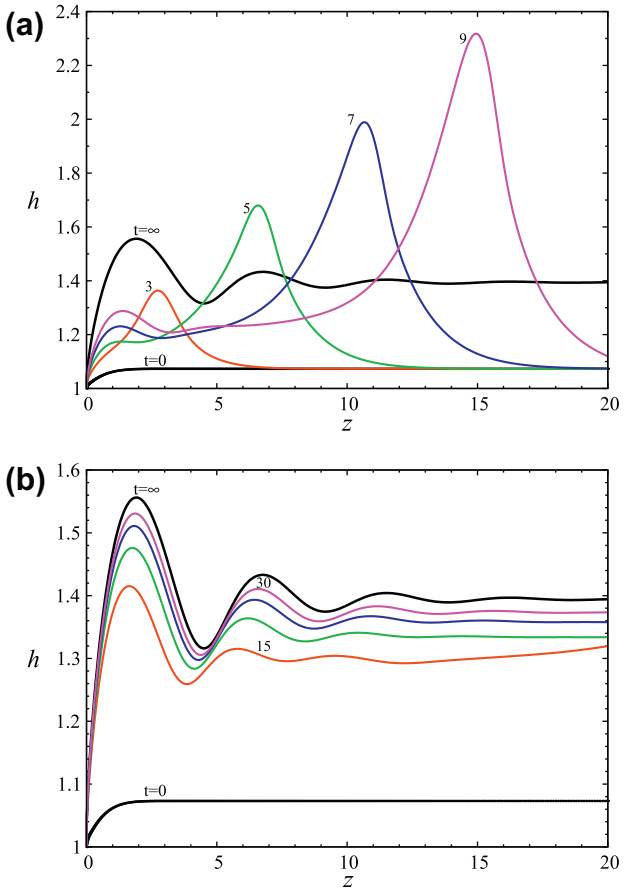

Fig. 14. Evolution of the free surface after perturbing the steady-state axisymmetric solution for $Re = 2$, $B = 0.06$, and $A = 0$ (no slip) from $Q_0 = 0.5$ to $Q_0 = 1$: (a) $t = 3$, 5, 7, and 9; (b) $t = 15$, 20, 25, and 30; the free surface pro_les at $t = 0$ and ∞ are also shown.

(a) In creeping flow as well as for moderate Reynolds numbers at which the Newtonian jet actually contracts, the extrudate-swell ratio increases with compressibility after passing from a small minimum.
(b) Slip at the wall tends to reduce swelling at low Reynolds numbers and contraction at higher Reynolds numbers, weakening the above minimum and moving it to the right.
(c) The exit correction factor increases monotonically with compressibility and its absolute value is reduced by wall slip.
(d) As the Reynolds number is increased, n_{ex} initially decreases and then passes through a minimum which is shifted to the left as the slip number is increased.
(e) In compressible flow, stable steady-states are observed at moderate Reynolds numbers in which the extrudate surface exhibits oscillations that decay downstream. The free-surface oscillations are suppressed by slip, as expected.
(f) The competition of slip and inertia at moderate slip and Reynolds numbers leads to interesting stable extrudate shapes.

Acknowledgement

The authors are indebted to the ERASMUS program (subprogram SOCRATES) for scientific visits to Cyprus related to this project.

References

[1] Hill DA, Hasegawa T, Denn MM. On the apparent relation between adhesive failure and melt fracture. J Rheol 1990;34:891–918.
[2] Piau JM, El Kissi N, Tremblay B. Influence of upstream instabilities and wall slip on melt fracture and sharkskin phenomena during silicones extrusion through orifice dies. J Non-Newtonian Fluid Mech 1990;34:145–80.
[3] Hatzikiriakos SG, Dealy JM. Wall slip of molten high density polyethylenes. II. Capillary rheometer studies. J Rheol 1992;36:703–41.
[4] Mitsoulis E. Annular extrudate swell of Newtonian fluids: effects of compressibility and slip at the wall. J Fluids Eng 2007;129:1384–93.
[5] Denn MM. Extrusion instabilities and wall slip. Ann Rev Fluid Mech 2001;33:265–87.
[6] Hatzikiriakos SG. Wall slip of molten polymers. Prog Polym Sci 2012;37:624–43.
[7] Neto C, Evans DR, Bonaccurso E, Butt HJ, Graig VSJ. Boundary slip in Newtonian liquids: a review of experimental studies. Rep Prog Phys 2005;68:2859–97.
[8] Silliman WJ, Scriven LE. Separating flow near a static contact line: slip at a wall and shape of a free surface. J Comp Phys 1980;34:287–313.
[9] Phan-Thien N. Influence of wall slip on extrudate swell: a boundary element investigation. J Non-Newtonian Fluid Mech 1988;26:327–40.
[10] Georgiou GC, Crochet MJ. Compressible viscous flow in slits with slip at the wall. J Rheol 1994;38:639–54.
[11] Georgiou GC, Crochet MJ. Time-dependent compressible extrudate-swell problem with slip at the wall. J Rheol 1994;38:1745–55.
[12] Guillope C, Hakim A, Talhouk R. Existence of steady flows of slightly compressible viscoelastic fluids of White-Metzner type around an obstacle. Commun Pure Appl Anal 2005;4:23–44.
[13] Vinay G, Wachs A, Agassant J-F. Numerical simulation of weakly compressible flows: the restart of pipeline flows of waxy crude oils. J Non-Newtonian Fluid Mech 2006;136:93–105.
[14] Hatzikiriakos SG, Dealy JM. Start-up pressure gradients in a capillary rheometer. Polym Eng Sci 1994;34:493–9.
[15] Beverly CR, Tanner RI. Compressible extrudate swell. Rheol Acta 1993;32:526–31.
[16] Georgiou GC. The compressible Newtonian extrudate-swell problem. Int J Numer Meth Fluids 1995;20:255–61.
[17] Park CB, Behravesh AH, Venter RD. Low density microcellular foam processing in extrusion using CO_2. Polym Eng Sci 1998;38:1812–23.
[18] Taliadorou E, Georgiou G, Mitsoulis E. Numerical simulation of the extrusion of strongly compressible Newtonian liquids. Rheol Acta 2008;47:49–62.
[19] Mitsoulis E, Georgiou GC, Kountouriotis Z. A study of various factors affecting Newtonian extrudate swell. Comput Fluids 2012;57:195–207.
[20] Taliadorou E, Georgiou GC, Alexandrou AN. A two-dimensional numerical study of the stick-slip extrusion instability. J Non-Newtonian Fluid Mech 2007;146:30–44.
[21] Russo G, Phillips TN. Numerical simulation of steady planar die swell for a Newtonian fluid using the spectral element method. Comput Fluids 2012;39:780–92.
[22] Harmon DB. Drop sizes from low-speed jets. J Franklin Inst 1955;259:519–22.
[23] Tillett JPK. On the laminar flow of a free jet of liquid at high Reynolds numbers. J Fluid Mech 1968;32:273–92.
[24] Tanner RI. Engineering rheology. 2nd ed. Oxford, UK: Oxford University Press; 2000.
[25] Naguib HE, Park CB, Reichelt N. Fundamental foaming mechanisms governing the volume expansion of extruded polypropylene foams. J Appl Polym Sci 2004;91:2661–8.
[26] Moraru CI, Kokini JL. Nucleation and expansion during extrusion and microwave heating of cereal foods. Comp Rev Food Sci Food Sav 2003;2:147–65.